INTERFACIAL AND BED SHEAR STRESSES IN SALINE WEDGES

by

Vassilios Dermissis[1], Member, Technical Chamber of Greece

and Emmanuel Partheniades[2], Member, A.S.C.E.

ABSTRACT

The shear stresses and the associated friction coefficients at the interface and at the bed of an arrested saline wedge have been studied experimentally together with the detailed flow structure. Interfacial stresses, evaluated from hot film anemometer measurements and actual velocity profiles, agree well with those based on the integration of the equations of motion while the simplified one-dimensional analysis gave considerably higher values. It was found that both the average interfacial friction coefficient, $\bar{f}_i$ and the average bed friction factor, $\bar{f}_o$ are best correlated with the dimensionless number, $ReFr^2$, where Re and Fr are the Reynolds number and the non-densimetric Froude number of the flow respectively, and with the relative density difference, $\Delta\rho/\rho$. The results are presented in two families of curves with $\Delta\rho/\rho$ as a parameter. The scattering of data points is minimal and the agreement with the results of some previous laboratory investigations and field data is good.

1. INTRODUCTION

Shear stresses at the interface and at the bed of arrested or quasi-stationary saline wedges develop as a result of the flow pattern which is generated by the dynamic interaction of fresh and salt water. These stresses, noted by τ_i and τ_o respectively, as well as the associated coefficients, f_i and f_o, have been extensively studied in the past not only for saline wedges but also for other types of two-layered stratified flows (3). In particular, the frictional resistance at the interface and the related flow dynamics constitute two of the most intricate and most important aspects of stratified flows. A reasonable evaluation of the interfacial friction may lead

---

[1] Lecturer, Dept. of Civil Engrg., Aristoteles University of Thessaloniki, Greece.

[2] Prof., Dept. of Civil Engrg., Aristoteles University of Thessaloniki, Greece; and Prof., Dept. of Engrg. Sciences, University of Florida, Gainesville, Florida, U.S.A.

to a quantitative model, since stratified flow systems are controlled by gravity, friction, and inertia forces; they can, therefore, be readily analyzed to various degrees of approximation provided that suitable expressions for the friction forces at the interface and at the solid boundary are introduced. Two typical examples of such models are the one-dimensional analyses for uniform density underflows (6) and for arrested saline wedges (13).

In an earlier paper the authors reviewed studies on stratified flows prior to 1978 (4, 10). It was found that results obtained through various theories and equations differed enormously, and that the scattering of experimental data points in certain studies was too wide for the formulation of any reliable universal law (7, 8). The discrepencies were attributed to the restricting assumptions and conditions of each study and to the limited range of variation of the governing parameters while the scattering of data points suggested either that an inadequate number of independent variables was taken into consideration or that these variables were not properly separated in the dimensionless correlation parameters for their effect on the friction coefficients to be sufficiently displayed. It, moreover, appears that turbulent exchange through the interface may take place to a degree sufficient for the generation of Reynolds stresses while the flow maintains its stratified appearance (11).

The authors, in their first attempt to derive a univeral functional relationship for the interfacial friction coefficient, conducted extensive experimental investigations in a closed rectangular duct where fresh water was flowing over a quasi-stagnant salt water layer at various salinities (4, 10). The analysis of the test data was based on a one-dimensional steady uniform flow model similar to that developed by Schijf and Schoenfeld for open channels (13). Attempts to correlate f_i with the Reynolds number, the densimetric Froude number, and the Keulegan number resulted, like in several earlier studies, in wide scattering with no consistent trend of variation. The Keulegan number is defined by the Eq.:

$$\theta = \frac{1}{V}\left(\nu\, g\, \frac{\Delta\rho}{\rho}\right)^{1/3} \qquad (1)$$

where V is the local average velocity in the moving layer, ρ is the density of the fresh water, $\Delta\rho$ is the density difference between fresh and salt water, g is the acceleration of gravity and ν is the kinematic viscosity assumed to be the same for both fluids.

The scattering was minimized and a consistent trend of variation was achieved when f_i was plotted against the parameter $ReFr^2$, where Re and Fr are the Reynolds number and the non-densimetric Froude number, with $\Delta\rho/\rho$ as an independent parameter. The family of curves, thus obtained, agrees reasonably well with reanalyzed data obtained by other investigators and with one data point from the Mississippi river. In the present study, a similar correlation was achieved for both $\overline{f}_i$ and $\overline{f}_o$ for saline wedges. The interfacial shear stresses were evaluated both directly from hot film anemometer measurements and from

an integration of the equation of motion over each layer along the same line used by Keulegan (7, 8).

2. THEORETICAL BACKGROUND

The interfacial friction coefficients, f_i, have been evaluated by the following four different approaches:

2.1 Direct Measurement Approach

This approach was based on directly measured velocity profiles and Reynolds stresses from which the interfacial shear stress was computed by the equation:

$$\tau_i = \mu \frac{du}{dy} - \rho\overline{u'v'} \tag{2}$$

In this equation, u is the local temporal mean velocity, y is the direction normal to the flow direction, x, u' and v' are the instantaneous turbulent velocity components in the x and y directions respectively, and μ is the dynamic viscosity. From Eq. 2 the local interfacial friction factor, f_i, is defined as:

$$f_i = \frac{8\tau_i}{\rho V_1^2} \tag{3}$$

where V_1 is the average fresh water velocity (Fig. 1).

2.2 Integration of the Equations of Motion

In this approach the equations of motion were integrated for each layer in the vertical and in the horizontal directions over the salinity intrusion length.

The general two-dimensional equations of motion and continuity for steady flow have the forms:

$$u\frac{\partial u}{\partial x} + v\frac{\partial u}{\partial y} = -g\frac{dz_o}{dx} - \frac{1}{\rho}\frac{\partial p}{\partial x} + \frac{1}{\rho}\left(\frac{\partial \tau_{zx}}{\partial z} + \frac{\partial \tau_{yx}}{\partial y}\right) \tag{4}$$

and

$$\frac{\partial u}{\partial x} + \frac{\partial v}{\partial y} = 0 \tag{5}$$

where, refering to Fig. 1, u and v are the local temporal mean velocities in the x and y direction respectively, z is the horizontal direction normal to x-y plane, z_o is the bed elevation and τ_{zx} and τ_{yx} are the shear stresses in the direction x, acting on planes normal to z and y directions repectively.

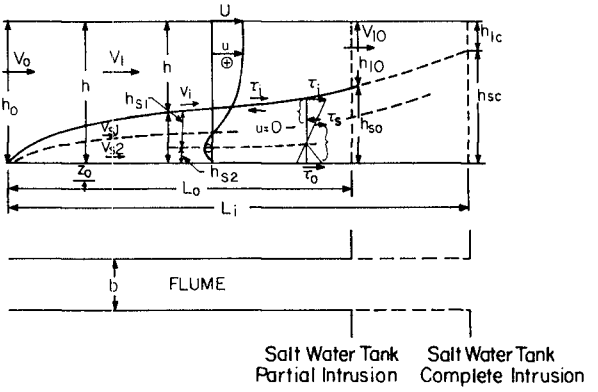

Fig. 1. Definition sketch of an arrested saline wedge.

A combinaton of Eqs. 4 and 5 leads to:

$$\frac{\partial u^2}{\partial x} + \frac{\partial (uv)}{\partial y} = -g \frac{dz_o}{dx} - \frac{1}{\rho} \frac{\partial p}{\partial x} + \frac{1}{\rho}\left(\frac{\partial \tau_{zx}}{\partial z} + \frac{\partial \tau_{yx}}{\partial y}\right) \qquad (6)$$

The last equation is first integrated over the cross sectional area of each layer separately and subsequently over the length of intrusion. In the second integration two cases had to be considered: 1) the case where the depth near the salt water basin is critical and the salinity intrusion length attains its maximum value, L_i and 2) the case where the fresh water depth near the basin is larger than critical, whereas the intrusion length, L_o, is less than L_i. In all experiments a layer of fresh water was formed over the salt water basin. As long as the depth of that layer was smaller than the critical depth of fresh water at the channel entrance, it had no effect on the salinity intrusion which attained its maximum length, L_i; otherwise, the actual intrusion length was equal to the distance from the toe of the wedge to the point where the fresh water depth is equal to that over the basin.

2.2.1. Complete intrusion.

2.2.1.1 Fresh water layer

The pressure distribution in that layer is given by

$$p = p_o + \rho g(h - y) \quad \text{for } y \geq h_s \qquad (7)$$

where $h = h_1 + h_s$ (Fig. 1) and where the vertical direction y is measured from the bottom. Eq. 6 is next integrated over the cross sectional area bh_1. Setting:

$$\alpha V_1^2 A_1 = \iint_{A_1} u^2 dA \tag{8}$$

where α is the momentum flux correction coefficient, neglecting the velocity variation in the z direction and taking into consideration the Leibnitz rule, integration of the first term of the left hand member yields:

$$\int_{-\frac{b}{2}}^{\frac{b}{2}} dz \int_{h_s}^{h} \frac{\partial u^2}{\partial x} dy = \frac{\alpha}{2} bh_1 \frac{dV_1^2}{dx} - bU^2 \frac{dh}{dx} + bV_i^2 \frac{dh_s}{dx} \tag{9}$$

where U and V_i are the velocities at the free surface and at the interface, respectively. Likewise:

$$\int_{-\frac{b}{2}}^{\frac{b}{2}} dz \int_{h_s}^{h} \frac{\partial (uv)}{\partial y} dy = bU^2 \frac{dh}{dx} - bV_i^2 \frac{dh_s}{dx} - bV_i v_s \tag{10}$$

where v_s is the net rate of salt water entrainment. The vertical velocity at the free surface is:

$$v_h = U \frac{dh}{dx} \tag{11}$$

and the same velocity at the interface was taken as:

$$v_{hs} = V_i \frac{dh_s}{dx} + v_s \tag{12}$$

The integrated terms of the right hand member of Eq. 6 are:

$$\int_{-\frac{b}{2}}^{\frac{b}{2}} dz \int_{h_s}^{h} g \frac{dz_o}{dx} dy = bh_1 g \frac{dz_o}{dx} \tag{13}$$

$$\frac{1}{\rho} \int_{-\frac{b}{2}}^{\frac{b}{2}} dz \int_{h_s}^{h} \frac{\partial p}{\partial x} dy = bh_1 g \frac{dh}{dx} \tag{14}$$

$$\frac{1}{\rho} \int_{h_s}^{h} dy \int_{-\frac{b}{2}}^{\frac{b}{2}} \frac{\partial \tau_{zx}}{\partial z} dz = -\frac{2h_1 \tau_w}{\rho} \tag{15}$$

$$\frac{1}{\rho}\int_{-\frac{b}{2}}^{\frac{b}{2}} dz \int_{h_s}^{h} \frac{\partial \tau_{yx}}{\partial y}\, dy = -\frac{1}{\rho}\, b\tau_i \tag{16}$$

where τ_w is the shear stress at the sidewalls. Eq. 6 obtains thus the form:

$$\frac{dH}{dx} + \frac{\alpha}{2g}\frac{dV_1^2}{dx} + \frac{1}{\rho g h_1}\left(\tau_i + \frac{2\tau_w h_1}{b}\right) + \frac{V_i v_s}{g h_1} = 0 \tag{17}$$

where H is the piezometric head, $z_o + h$, and $\frac{dH}{dx}$ is, therefore, the slope of the piezometric line. The entrainment velocity is equal to:

$$v_s = \frac{q_s}{b L_i} \tag{18}$$

where q_s is the rate of salt water entrainment over the saline wedge. The latter has been given by Keulegan (8). In the analysis of data, the term $V_i v_s / g h_1$ was found to be of minor importance with a maximum effect of 5%. Because of this reason and of the fact that entrainment takes place not continuously over the interface, but at isolated spots in the form of breaking of interfacial waves, it was neglected in the subsequent analyses. Expressing, next, τ_w by:

$$\tau_w = f_w \frac{\rho V_1^2}{8} \tag{19}$$

the following equation for τ_i is obtained:

$$\frac{\tau_i}{\rho} = -g(h - h_s)\frac{dH}{dx} - \frac{\alpha}{2}(h - h_s)\cdot\frac{dV_1^2}{dx} - \frac{f_w(h - h_s)V_1^2}{4b} \tag{20}$$

which, integrated for $-L_i$ to 0, gives:

$$\frac{T_i}{\rho V_o^2} = -g\frac{h_o}{V_o^2}\overline{\frac{dH}{dx}}\, I_1 - \frac{\alpha h_o}{2L_i} I_2 - \frac{f_{wo} h_o}{4b} I_3 \tag{21}$$

where T_i and $\overline{dH/dx}$ are the average values of τ_i and of dH/dx over the wedge and where I_1, I_2 and I_3 are the following dimensionless functions:

$$I_1 = \int_{-1}^{0} \left(\frac{h}{h_o} - \frac{h_s}{h_o}\right) d\left(\frac{x}{L_1}\right) \tag{22}$$

$$I_2 = \int_{-1}^{0} \frac{1}{V_o^2} \frac{dV_1^2}{d\left(\frac{x}{L_1}\right)} \left(\frac{h}{h_o} - \frac{h_s}{h_o}\right) d\left(\frac{x}{L_1}\right) \tag{23}$$

$$I_3 = \int_{-1}^{0} \frac{f_w}{f_{wo}} \left(\frac{V_1}{V_o}\right)^2 \left(\frac{h}{h_o} - \frac{h_s}{h_o}\right) d\left(\frac{x}{L_1}\right) \tag{24}$$

For the evaluation of these integrals, the following dimensionless equations for the interface, developed by the authors and Mehta and based on Schijf and Schoenfeld's model (11, 13), was used:

$$\frac{x}{L_1} = \frac{\left(\frac{h_s}{h_{sc}}\right)^3 \left\{\left[4 - 2\frac{h_s}{h_{sc}}\left(1-(F_o')^{2/3}\right)\right]^2 + \left[4 + \frac{h_s}{h_{sc}}\left(1-(F_o')^{2/3}\right)\right]\right\}}{6(F_o')^{4/3} + 3(F_o')^{2/3} + 1} + \\ - \frac{10\left(\frac{h_s}{h_{sc}}\right)^2 \left[(F_o')^{4/3} + (F_o')^{2/3} + 1\right]}{6(F_o')^{4/3} + 3(F_o')^{2/3} + 1} + 1 \tag{25}$$

where $F_o' = V_o\sqrt{g(\Delta\rho/\rho)h_o}$ is the densimetric Froude number with V_o and h_o defined in Fig. 1. The three integrals obtain thus the form:

$$I_1 = \frac{2\left[5(F_o')^2 + 6(F_o')^{4/3} + (F_o')^{2/3} + 1\right]}{3\left[6(F_o')^{4/3} + 3(F_o')^{2/3} + 1\right]} \tag{26}$$

$$I_2 = 2\left[(F_o')^{-2/3} - 1\right] \tag{27}$$

$$I_3 = \frac{0.29\left[5 + 255(F_o')^{13/6} - 221(F_o')^2 - 39(F_o')^{17/6}\right]}{\left[1 - (F_o')^{2/3}\right]^3 \cdot \left[6(F_o')^{4/3} + 3(F_o')^{2/3} + 1\right]} \tag{28}$$

2.2.1.2 Salt water layer

A similar integration of Eq. 6 over the cross sectional area of the wedge, $A_s = bh_s$, with the pressure this time described by the equation:

$$p = p_o + (h - h_s)\rho g + g(\rho + \Delta\rho)(h_s - y) \tag{29}$$

gives:

$$\frac{\tau_i + \tau_o}{g(\rho + \Delta\rho)h_s} = \frac{\rho}{\rho + \Delta\rho} \cdot \frac{dH}{dx} + \frac{\Delta\rho}{\rho + \Delta\rho} \cdot \frac{d(h_s + z_o)}{dx}$$

$$+ \frac{\beta}{gh_s} \frac{d(V_i^2 h_s)}{dx} + \frac{V_i v_s}{gh_s} = 0 \tag{30}$$

where β is the momentum flux correction coefficient for the lower layer given in terms of V_i by:

$$\beta V_i^2 A_s = \iint_{A_s} u^2 dA \tag{31}$$

and where the sidewall friction has been neglected since, due to the reversal of flow direction, its overall effect is expected to be negligible . Integration of Eq. 30 from $-L_i$ to 0 gives:

$$\frac{T_i}{\rho V_o^2} + \frac{T_o}{\rho V_o^2} = \frac{gh_o}{V_o^2} \overline{\frac{dH}{dx}} I_4 + \frac{g\frac{\Delta\rho}{\rho}}{2V_o^2 L_i} h_{sc}^2 + \frac{\rho \frac{\Delta\rho}{\rho} h_o}{V_o^2} \cdot \overline{\frac{dz_o}{dx}} I_4$$

$$+ \beta\left(1 + \frac{\Delta\rho}{\rho}\right) \left(\varepsilon \frac{V_{ic}}{V_o}\right)^2 \cdot \frac{h_{sc}}{L_i} \tag{32}$$

where T_o is the average bed shear stress over the length of intrusion, $\overline{dz_o/dx} = -S_o$ is the average bottom slope, $h_{ic} = h - h_{sc}$ is the critical depth of the fresh water layer, and $\varepsilon = V_i/V_o$. The term $V_i v_s/gh_s$ has again been neglected for the aforementioned reasons while the integral I_4 is:

$$I_4 = \int_{-1}^{0} \frac{h_s}{h_o} d\left(\frac{x}{L_i}\right) \tag{33}$$

which, on the basis of Eq. 25, becomes:

$$I_4 = \frac{\left[1 - (F_o')^{2/3}\right] \cdot \left[10(F_o')^{4/3} + 4(F_o')^{2/3} + 1\right]}{3\left[6(F_o')^{4/3} + 3(F_o')^{2/3} + 1\right]} \cdot \qquad (34)$$

The analysis presented so far is similar to the one used by Keulegan (7, 8) with the following differences: 1) A more detailed analytical equation for the wedge profile has been used instead of one single experimental curve and, 2) the actual measured values of α and β for each experiment were used, instead of the constant values of $\alpha = 1.028$ and $\beta = 0.146$ used by Keulegan.

2.2.2 Partial intrusion

In several experiments, the fresh water layer at the downstream basin was larger than h_{1c} - in which case the salt water depth at the downstream end of the channel, h_{so}, was smaller than h_{sc} (Fig. 1). In these cases the following simplified form of Eqs. 21 and 32 was derived and used: First, Eqs. 20 and 30 are written in the form:

$$\frac{\tau_i}{\rho V_o^2} = -\frac{gh_1}{V_o^2}\frac{dH}{dx} - \frac{\alpha h_o}{V_o}\frac{dV_1}{dx} - \frac{f_w h_1 V_1^2}{4bV_o^2} \qquad (35)$$

$$\frac{\tau_i}{\rho V_o^2} + \frac{\tau_o}{\rho V_o^2} = \frac{gh_s}{V_o^2}\frac{dH}{dx} + \frac{(\frac{\Delta\rho}{\rho})gh_s}{V_o^2} \cdot \frac{dh_s}{dx} + \frac{\beta(1+\frac{\Delta\rho}{\rho})^2 \varepsilon^2}{V_o^2} \cdot \frac{d(V_1^2 h_s)}{dx} \qquad (36)$$

where dz_o/dx in Eq. 32 has been neglected as much smaller in comparison to dh_s/dx and where the wall friction coefficient f_w has been introduced by the Blasius equation:

$$f_w = \frac{0.316}{Re^{0.25}} \qquad (37)$$

where the Reynolds number, Re is:

$$Re = \frac{4V_1 R_{h1}}{\nu} \qquad (38)$$

and

$$R_{h1} = \frac{bh_1}{(b + 2h_1)} \qquad (39)$$

Eq. 35 obtains thus the form:

$$\frac{\tau_i}{\rho V_o^2} = -\frac{gh_1}{V_o^2}\frac{dH}{dx} - \frac{\alpha h_o}{V_o}\frac{dV_1}{dx} - \frac{0.0559}{b^{1.25}} h_o^2 \left(\frac{\nu}{V_o h_o}\right)^{0.25} \left[\frac{(b + 2h_1)^{0.25}}{h_1}\right] \qquad (40)$$

Averaging of Eqs. 36 and 40 over the actual length of salinity intrusion, L_o, as in the case of full intrusion, but considering h_1 and h_s constant and equal to their average values $\bar{h}_1$ and $\bar{h}_s$, leads to the following equations:

$$\frac{T_i}{\rho V_o^2} = -\frac{g\bar{h}_1}{V_o^2}\frac{d\bar{H}}{dx} - \frac{\alpha h_o}{h_{1_o}} \cdot \frac{h_{so}}{L_o} - \frac{0.0559}{b^{1.25}} h_o \left(\frac{\nu}{V_o h_o}\right)^{0.25} \left[\frac{(b + 2h_1)^{0.25}}{h_1}\right] \tag{41}$$

and

$$\frac{T_1}{\rho V_o^2} + \frac{T_o}{\rho V_o^2} = \frac{g\bar{h}_s}{V_o^2} \cdot \frac{d\bar{H}}{dx} + \frac{\left(\frac{\Delta\rho}{\rho}\right)g}{2V_o^2} \cdot \frac{h_{so}^2}{L_o} + \frac{\beta\left(1 + \frac{\Delta\rho}{\rho}\right)\varepsilon^2 V_{1_o}^2}{V_o^2} \cdot \frac{h_{so}}{L_o} \tag{42}$$

where bars indicate average values over the length L_o. For a direct evaluation of the average stresses T_1 and T_o, given either by Eqs. 21 and 32 or by 41 and 42, a reliable measurement of the average slope of the piezometric line, $d\bar{H}/dx$, is required - as was done earlier by Keulegan (7, 8). This has been found to be very difficult, since the head loss over the effective length of the flume is of the order of a few tenths of a millimeter. Attempts to measure that head loss optically through a laser beam required an excessively long time of measurement, due primarily to the slowness of achieving equilibrium in the two static tanks, and to the very long period of oscillation of the water level in these tanks. Moreover, the above equations are quite sensitive to $d\bar{H}/dx$ so that a measurement error of the order of 10% may cause an error in T_1 of the order of 50% (5). This difficulty was bypassed by introducing a linear relationship between τ_1 and τ_o. Indeed, the shear stress distribution within the wedge is given by the equation.

$$\frac{\partial\tau}{\partial y} = \frac{\partial}{\partial x}\left[p + g(\rho + \Delta\rho)z_o + (\rho + \Delta\rho)\frac{u^2}{2}\right] \tag{43}$$

The velocity head is very small and can be neglected. Eq. 29 then, for p gives:

$$\frac{\partial\tau}{\partial y} = \rho g \frac{dH}{dx} + (\Delta\rho)g \frac{\partial(h_s + z_o)}{\partial x} \tag{44}$$

The free surface slope, dH/dx, is very small, as discussed, and can be considered as constant. Also, apart from two relatively short segments around the wedge toe and the critical section, the interface is very nearly a plane surface, and $d(h_s + z_o)/dx$ is also very nearly constant. Therefore, it is reasonable to assume linear variation of τ with y within the wedge. It follows thus from Fig. 1 that:

$$\frac{\tau_i + \tau_o}{\tau_i} = \frac{h_s}{h_{s1}} = \lambda \tag{45}$$

where h_{s1} is the distance from the interface to the point of maximum velocity in the wedge. It was assumed next that λ is constant over the wedge - in which case Eq. 45 holds also for the average stresses T_i and T_o, that is:

$$T_i + T_o = \lambda T_i \tag{46}$$

Eliminating $d\bar{H}/dx$ from Eqs. 41 and 42 and using the last relationship, the following equation is obtained:

$$\frac{T_i}{\rho V_o^2} = \left\{ \frac{\left[\left(\frac{\Delta\rho}{\rho}\right) g h_{so} + 2\beta\left(1 + \frac{\Delta\rho}{\rho}\right)\varepsilon^2 V_{1o}^2\right] h_{1o}\bar{h}_1 - 2\alpha h_o \bar{h}_s V_o^2}{2V_o^2 h_{1o}(\lambda\bar{h}_1 + \bar{h}_s)} \right\} \frac{h_{so}}{L_o} +$$

$$- \frac{0.0559}{b^{1.25}} h_o^2 \left(\frac{\nu}{V_o h_o}\right)^{0.25} \cdot \left[\frac{(b + 2h_1)^{0.25}}{h_1}\right] \cdot \frac{\bar{h}_s}{(\lambda\bar{h}_1 + \bar{h}_s)} \tag{47}$$

All the terms of the right hand member of Eq. 47 are either known or can be directly measured. The maximum measurement error of λ was estimated to be about 15% (5). With T_i computed from Eq. 47, T_o is readily evaluated from Eq. 46. $d\bar{H}/dx$ could be eliminated in the same way from Eqs. 21 and 32, valid for complete intrusion. However, after a few trials for the latter case, it was found that Eqs. 41 and 42 could be used for both partial and complete intrusion. These equations have been used for the analysis of all data.

2.3 One-dimensional Energy Equation

This equation, developed by Schijf and Schoenfeld (13), is based on the energy conservation principle applied separately to each layer and on the assumptions of one-dimensional flow, infinite width, and negligible entrainment through the interface. For zero net flow within the wedge, the average velocity is also zero and, therefore, for the one dimensional approach, τ_o has to be taken also as zero. The final form of the equation is:

$$\bar{f}_i = \frac{2h_o}{L_i}\left[\frac{1}{5(F_o')^2} - 2 + 3(F_o')^{2/3} - \frac{6}{5}(F_o')^{4/3}\right] \tag{48}$$

which gives the average interfacial friction factor if the total intrusion length is measured. If the actual intrusion length, L_o, is less than L_i, the latter can be computed graphically from Eq. 25, where h_{sc} is known and equal to $h_o[1 - (F_o')^{2/3}]$ (11).

2.4 Simplified Equations of Motion

This is a combination of the last two approaches and its main objective was to investigate the effect of the assumption of zero bed shear stress and zero wall stress, used in the one-dimensional model, on the interfacial shear. For $\tau_o = 0$, $\lambda = 1$, $f_w = 0$ and $\beta = 0$, Eq. 47 reduces to the approximate form:

$$\frac{T_i}{\rho V_o^2} = \left[\frac{(\frac{\Delta\rho}{\rho}) g \bar{h}_1 h_{so}}{2V_o^2 h_o} - \frac{\alpha \bar{h}_s}{\bar{h}_{1_o}} \right] \cdot \frac{h_{so}}{L_o} \qquad (49)$$

3. BASIC RESEARCH EQUIPMENT

The experiments were conducted in a variable slope plexiglass flume 20 m long, 46 cm wide, and 46 cm deep, constructed at the Coastal Engineering Laboratory of the University of Florida. This flume, outlined in Fig. 2, discharges into a 3 m by 1.53 m tank supported on another 3 x 3 x 0.75 m^3 tank.

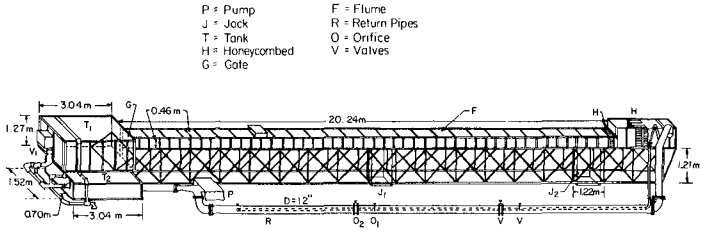

Fig. 2. Outline of basic experimental apparatus.

The channel is connected at its upstream end to a 2.31 m by 0.45 m head tank where the fresh water is pumped into from the fresh water tank and where turbulence dampens out through a honeycombed section. The water circulation system consists of an axial flow pump, of two pipes with either one or both in operation, depending on the required discharge, and of all the necessary orifice meters, valves, gates, pressure taps and manometers. The maximum discharge is about 115 l/sec.

The channel and head tank are supported on a steel frame 1.2 m high, which rests on two hydraulic jacks - one at the center and the other at the upstream end of the flume. Through a gear-chain system, the central jack could be moved up and down at a distance equal to $\frac{1}{2}$ that of the upstream jack. The $\frac{1}{2}$-inch thich plexiglass wall of the flume forms a channel with its flanges, fortified with stiffeners, directed outwards. To this steel frame, rails have been placed on

each of the upper two flanges for the support and smooth movement of the instrument carriage. The downstream end of the channel is connected to the salt water tank through a five centimeter long thick rubber forming a flexible and waterproof hinge. A water-tight vertical plexiglass gate separates the flume from the salt water tank. That gate can be raised and lowered mechanically by a vertical threaded shaft and a circular threaded disc supported on an independently fixed frame. A second gate at the downstream end of the salt water tank regulates the water level in the latter. The outlined system of flume and tanks is supplemented with the necessary pipes and valves for proper operation and control.

The measuring instruments - that is, the hot film anemometers, a specially designed salinity probe, and the point gages - are supported on the aforementioned carriage, which is collapsable sidewise to permit its movement over the cross bars of the flume without removing the instruments.

4. EXPERIMENTAL RESULTS

After the necessary preparations and instrument calibration, each experiment was started and continued to a point where reasonable steady state conditions were established. Entrainment caused a gradual erosion of the salt water layer as a result of which salt water had to be periodically supplied from the preparation tank to the salt water basin. Space limitations do not permit a description of the detailed procedures of experimentation and calibration, which can be found in ref. (5) and in a forthcoming report. The measurements took place immediately after the steady state was achieved and lasted for about one-half hour, during which no measurable change in the flow conditions occurred. The primary measurements consisted of velocity and density profiles - with points more densely located around the interface. The instantaneous velocities were recorded on tapes from which the Reynolds stresses were subsequently computed. A total of 74 experiments were conducted with fully developed turbulent flows. The relative density difference, $\Delta\rho/(\rho + \Delta\rho)$, in these experiments ranged from 0.008 to 0.093. In such flows the velocity distribution in the neighborhood of the interface was found to be logarithmic and quite similar to that near solid boundaries. This is in general agreement with results from earlier studies (2, 9) but with major differences in certain important aspects. The velocity distribution laws and the flow structure around the interface is the subject of another forthcoming paper. It was found that the salinity distribution around the interface follows closely the law:

$$\frac{\rho_\ell - \rho}{\Delta\rho} = \frac{1}{2}\left[1 - \tanh\left(\frac{y - h_s}{\delta/2}\right)\right] \tag{50}$$

where ρ_ℓ is the local density, y is the distance from the bed, h_s is the depth of the density interface, and δ is the thickness of the interfacial zone, as defined in Fig. 3.

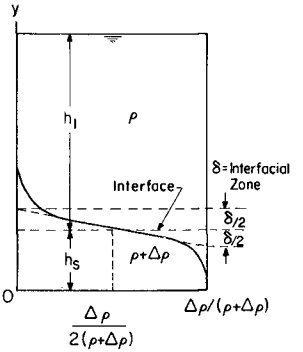

Fig. 3 Definition sketch for the interfacial zone.

As determined in an earlier study by the authors (4, 10), it was again found that the best correlation is obtained if f_i, determined by any one of the outlined four methods, is plotted against the dimensionless number $ReFr^2$ with $\Delta\rho/(\rho + \Delta\rho)$ as an independent parameter, where:

$$Re = \frac{4\overline{V}_1 R_h}{\nu}, \quad Fr^2 = \frac{V_1^2}{gR_h} \tag{51}$$

and where R_h is the hydraulic radius of the fresh water layer. The parameter $ReFr^2$ can be written in the form:

$$ReFr^2 = \frac{4\overline{V}_1^3}{g\nu} = \frac{4V_o^3 I_R}{g\nu} \tag{52}$$

where:

$$I_R = \frac{10}{\left[6(F_o')^{4/3} + 3(F_o')^{2/3} + 1\right]} \tag{53}$$

In Fig. 4 the results for four of the eight ranges of $\Delta\rho/(\rho + \Delta\rho)$ computed by all four approaches are shown with the average value of $\Delta\rho/(\rho + \Delta\rho)$ for each range indicated at the insert. The results from all four approaches can thus be compared. Here the interfacial friction coefficient is defined either as:

$$f_i = \frac{8\tau_i}{\rho\overline{V}_1^2} \tag{54}$$

or as:

$$\bar{f}_i = \frac{8T_i}{\rho \bar{V}_1^2} \tag{55}$$

with T_i computed from Eq. 47 for the second approach and from Eq. 49 for the fourth approach. In the third approach $\bar{f}_i$ was evaluated from Eq. 48. The comparison of these four sets of data leads to the following conclusions:

First, as in the earlier study by the authors (4, 10), the scattering of data points around each curve is minimal for a flow of this type. Secondly, there is a very good agreement between the data obtained from the first two approaches - that is, between the data based on direct shear stress measurements and those based on the integration of the equations of motion. These data constitute the lower family of curves. Thirdly, there is an equally good agreement between the results based on the two approximate approaches and which constitute the upper family of curves (dotted lines). Finally, a comparison of the two families of curves indicates that both approximate approaches give values of f_i considerably higher than the corresponding values obtained either by direct measurments or through the equations of motion. This difference is indicative of the effect of neglecting the bed shear stresses. It follows that $\bar{f}_i$, as determined from Eq. 48 through calibration, that is, by measuring L_i either in the laboratory or in the field (11), can be used as a convenient virtual friction coefficient for modeling purposes; it is not representative of the true shear stress at the interface, however.

The above conclusions hold also for the case of $\Delta\rho/(\rho + \Delta\rho)$ equal to 0.0225, 0.0355, 0.0485 and 0.082. For this reason the data for these cases are not reproduced in detail; instead, the summary of all eight curves based on the first and second approach is given in Fig. 5.

In Fig. 6 the curve corresponding to $\Delta\rho/(\rho + \Delta\rho) = 0.0225$ has been reploted together with reanalyzed laboratory data by Abraham and Eysink (1) and with one field data point from the Mississippi estuary (11). The agreement is quite good. This suggest that until the curves of Fig. 5 are implemented with field data, they can be tentatively extrapolated following the extrapolation of the 0.0225 curve of Fig. 6.

In Fig. 7, the results for $\Delta\rho/(\rho + \Delta\rho) = 0.0225$ are compared with resent results obtained by Powell for flow of fresh water over a semistagnant deep water layer in an open conduit and for a relative density difference close to 0.024 (12). When plotted against the Reynolds number only, these two sets of data deviate strongly (Fig. 7a); however, they appear to closely agree when they are plotted against $ReFr^2$. In fact, the drop of the curve for low values of $ReFr^2$ agrees with the trend observed in the authors' experiments. Thus, Powell's point for Re≈22000, which in his original diagram (Fig. 7a) seems to be in error, is in fact in agreement with the general law derived from this study.

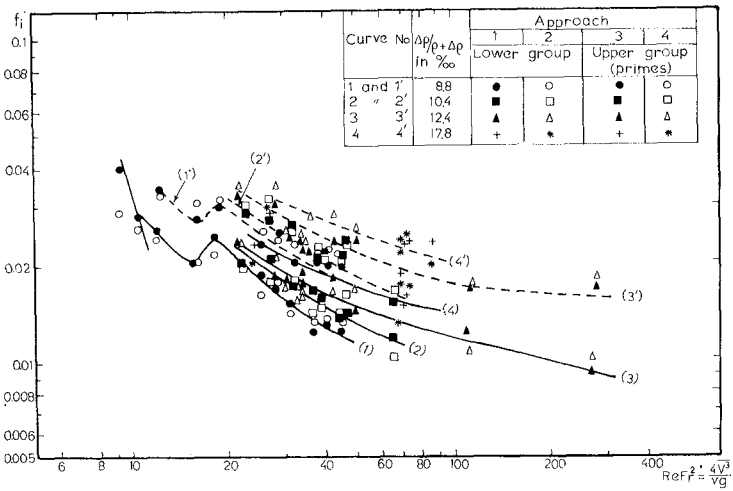

Fig. 4. Interfacial friction coefficients obtained from all four approaches.

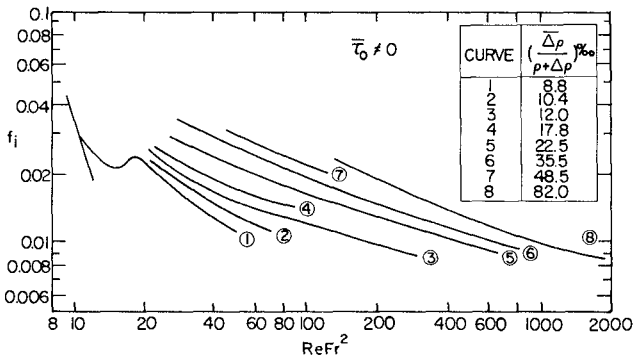

Fig. 5. Summary of interfacial friction coefficient curves based on approaches (1) and (2).

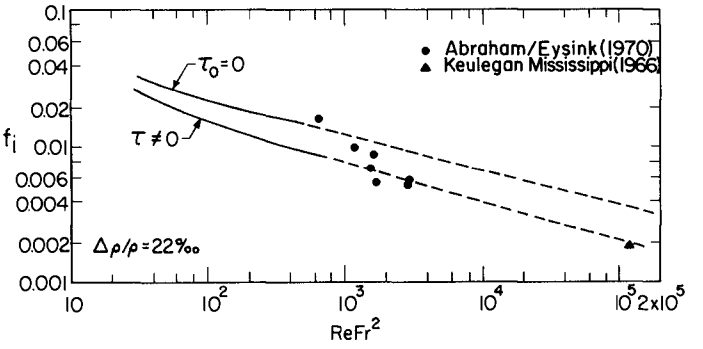

Fig. 6 Comparison of results of the present study with test data of previous studies.

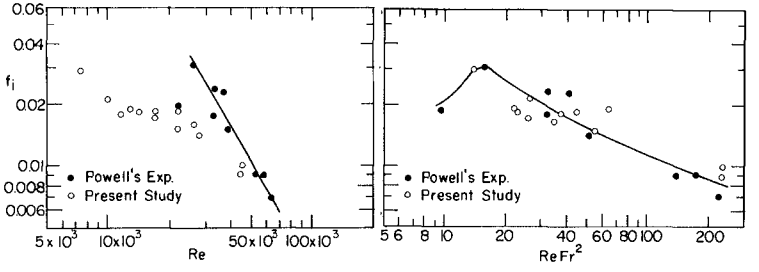

a. Plot vs Re b. Plot vs $ReFr^2$

Fig. 7 Comparison of results of present study with Powell's data (12).

The bed friction coefficient, f_o, defined as:

$$f_o = \frac{8T_o}{\rho \bar{V}_1^2} \tag{56}$$

has been determined from Eq. 46 where $T_1 = \tau_1$ was computed from Eq. 54 for values of f_1 taken from Fig. 5. The value of λ was determined for each experiment and the results are shown in Fig. 8. λ appears to be a function of the number $ReFr^2$ only while for values of the latter smaller than 100, it is essentially constant and equal to about 1.4. The results are plotted in Fig. 9 as a family of curves similar to the

one of Fig. 6. It is observed that, contrary to conclusions of earlier studies (7, 8), f_o is clearly smaller than the corresponding f_i.

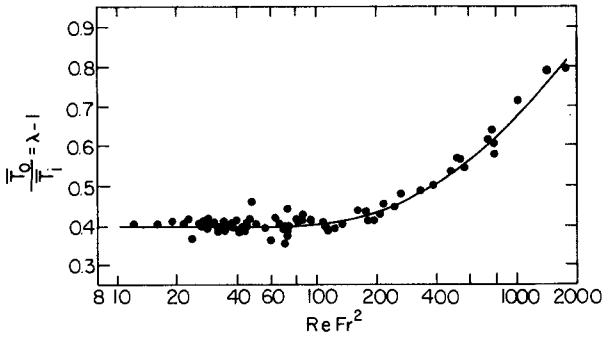

Fig. 8 Variation of $\lambda = \tau_i/\tau_o$ with $ReFr^2$.

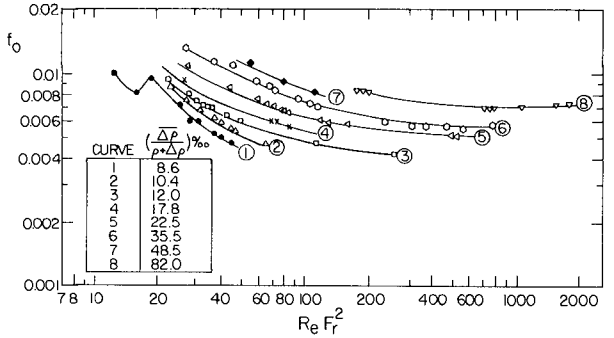

Fig. 9. Bed friction coefficients, f_o.

5. SUMMARY AND CONCLUSIONS

Laboratory experiments and theoretical analyses led to a new relationship linking the friction coefficients at the interface and at the bed of arrested saline wedges to the pertinent flow parameters and fluid properties. The relationships are presented graphically as a family of curves with $ReFr^2$ as an abscissa and the relative density difference, $\Delta\rho/(\rho + \Delta\rho)$, as an independent parameter. The scattering of data points was minimal and much lower than in earlier studies on the subject. In the present correlations the number $ReFr^2$ incorporates the friction, gravity, and inertia forces, which control the main flow, while the buoyant forces, which are responsible for the

density stratification and the asociated flow pattern have been separated and introduced through the parameter $\Delta\rho/(\rho + \Delta\rho)$.

This study indicated that values of f_i evaluated through an integration of the equations of motion closely agree with values based on measured velocity profiles and Reynolds stresses. Values of f_i obtained from the simplified and frequently used Schijf-Schoenfeld's one-dimensional analysis were shown to be higher than corresponding values based on the previous two methods.

ACKNOWLEDGEMENTS

This study has been supported by the U.S. National Science Foundation under Grant No. ENG 76-11537-A01. Travel funds were provided to the second author by the same institution under Grant No. CEE - 8214607 for presentation of this paper before the 18th International Conference on Coastal Engineering in Cape Town, South Africa. Both supports are gratefully acknowledged.

REFERENCES

1. Abraham, G. and Eysink, W.D., "Magnitude of Interfacial Shear in Exchange Flow," Journal of Hydraulic Research, I.A.H.R., Vol. 9, No. 2, 1971.

2. Csanady, G.T., "Turbulent Interface Layers," Journal of Geophysical Research, Vol. 83, No. C5, 1978, pp. 2329-2342.

3. Delft Hydraulics Laboratory, "Momentum and Mass Transfer in Stratified Flows," Report on Literature Study, R880, Delft, Netherlands, 1974.

4. Dermissis, V., "A Study of the Interfacial Friction Coefficient in a Two-layered Fluid System," (in Greek) Dissertation for the Degree of Doctor in Civil Engineering, School of Engineering, Aristotoles University of Thessaloniki, Greece, 1977.

5. Dermissis, V., "A Study of the Interfacial and Bed Shear Stresses in an Arrested Saline Wedge and of the Interfacial Flow Structure," (in Greek) Professorial (Dozent) dissertation, School of Engineering, Aristoteles University of Thessaloniki, Greece, 1982.

6. Ippen, A.T. and Harleman, D.R.F., "Steady State Characteristics of Subsurface Flows," Circular No. 521 "Gravity Waves", U.S. Dept. of Commerce National Bureau of Standards, 1952.

7. Keulegan, G.H., "Significant Stresses of Arrested Saline Wedges," Rept. No. 4267, National Bureau of Standards, August, 1955.

8. Keulegan, G.H., "The Mechanics of an Arrested Saline Wedge," Ch. 11, Estuary and Coastline Hydrodynamics, edited by A.T. Ippen, McGraw-Hill, 1966.

9. Lofquist, K., "Flow and Stress Near an Interface between Stratified Liquids," The Phys. of Fluids, Vol. 3, No. 2, 1960, pp. 158-175.

10. Partheniades, E. and Dermissis, V., "Interfacial Friction Coefficients in a Two-layered Stratified Flow," Proceedings, 16th Coastal Engineering Conference, Hamburg, Germany, Vol. 3, Ch. 170, pp. 2778-2797.

11. Partheniades, E., Dermissis, V. and Mehta, A.J., "On the Shape and Interfacial Resistance of Arrested Saline Wedges," Proceedings, 15th Congress of I.A.H.R., Sao Paulo, Brazil, Vol. I, 1975, pp. 157-164.

12. Powell, G.M., "The Structure of Velocity and Density Interfaces in a Weekly Turbulent Stratified Shear Flow," A dissertation presented in partial fulfillment of the requirements for the degree of Doctor of Philosophy, University of Florida, 1979.

13. Schijf, J.B. and Schoenfeld, J.C., "Theoretical Considerations on the Motion of Salt and Fresh Water," Proceedings, Minn. Intern. Hydr. Conv., 1953, pp. 321-333.